Solid State Communications, Vol. 80, No. 6, pp. 439–445, 1991.
Printed in Great Britain.

0038–1098/91 $3.00 + .00
Pergamon Press plc

ELECTRON PARAMAGNETIC RESONANCE OF NICKEL IN SILICON – II. HYPERFINE AND QUADRUPOLE INTERACTIONS

N.T. Son*, A.B. van Oosten and C.A.J. Ammerlaan

Van der Waals-Zeeman Laboratorium der Universiteit van Amsterdam, Valckenierstraat 65,
NL-1018 XE Amsterdam, The Netherlands

(*Received* 15 *July* 1991 *by B. Mühlschlegel*)

An electron paramagnetic resonance (EPR) study on *n*-type silicon doped with nickel enriched to 88.1% ^{61}Ni is presented. The structure due to the ^{61}Ni isotope with nuclear spin $I = 3/2$ was investigated. The EPR spectrum with the appearance of "forbidden" lines can be described by a spin Hamiltonian including the nuclear Zeeman, hyperfine and quadrupole interaction terms. A computer calculation of energy levels and transition probabilities of all EPR transitions was made explaining the angular dependence of the magnetic field positions of the resonances and their intensities. The hyperfine tensor A, with principal values $A_{[100]} = 1.01$ MHz, $A_{[011]} = -39.98$ MHz and $A_{[0\bar{1}1]} = -37.60$ MHz, is nearly axial around [1 0 0]. An analysis of hyperfine and quadrupole interactions was carried out revealing the specific effect of the nickel impurity on the electronic structure of the centre. Based on the information about spin and charge density as derived in the analysis, a dihedral bonding model for the Si : Ni_s^- centre is supported.

1. INTRODUCTION

ELECTRON paramagnetic resonance (EPR) studies on substitutional transition metal impurities were reported a long time ago for the cases of palladium and platinum in silicon [1] and of nickel in germanium [2]. Just recently, an analogous spectrum was observed in *n*-type silicon doped with nickel [3]. Based on the observed hyperfine interaction with nickel isotope ^{61}Ni and investigations of the phosphorus concentration and illumination treatments on the spectrum [4], it is concluded that this EPR spectrum is related to a negative substitutional nickel. In this paper, we report the EPR observation of angular dependence patterns of line positions and line intensities, as well as the analysis of the hyperfine and quadrupole interactions with ^{61}Ni. This result is very similar to that of Pd_s^- in silicon and Ni_s^- in germanium. These experimental results are used for evaluating the validity of the models. In agreement with the EPR data, we propose the model for Ni_s^- in which the nickel atom bonds to two nearest silicon neighbours.

2. EXPERIMENTAL

Starting material for the preparation of samples was float zone, dislocation free, *n*-type, phosphorus doped silicon with the resistivity of about 8 Ωcm at room temperature. The typical dimensions of the samples are 15 mm × 1.5 mm × 1.5 mm with the length along the [0 1 1] crystal direction. Pieces of nickel enriched to 88.1% ^{61}Ni were scratched on the surfaces of the sample, and the diffusion was made in a closed quartz ampoule containing 200 mbar of Ar. After 16 h of diffusion at 1200 °C, the whole ampoule was immediately immersed in water. The EPR measurements were performed on a superheterodyne spectrometer at the microwave frequency of about 23 GHz (K-band) and in the dispersion mode. The sample was mounted with the [0 1 1] direction perpendicular to the plane of rotation of the magnetic field. The measurements were taken with the sample at liquid helium temperature.

3. EPR RESULTS AND ANALYSIS

3.1. *EPR spectrum*

The sample mentioned above was measured at the microwave frequency $\nu = 23.2909$ GHz. The spectrum as described in Refs. [3] and [4], which was identified as arising from substitutional nickel impurity in the negative charge state, was observed. The resonances are due to the non-magnetic nickel isotopes (^{58}Ni, ^{60}Ni, ^{62}Ni and ^{64}Ni) which are present to the total

---

* Permanent address: Department of Physics, University of Hanoi, Vietnam.

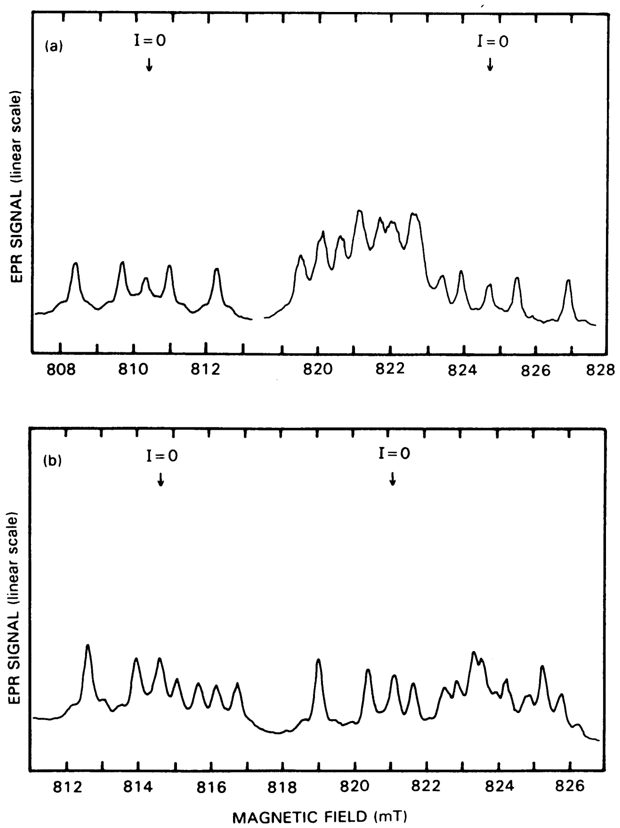

Fig. 1. EPR spectrum of Si:^{61}Ni$_s^-$: for (a) **B** || [0 1 1] and (b) **B** is 18° away from [1 0 0], showing the appearance of forbidden lines.

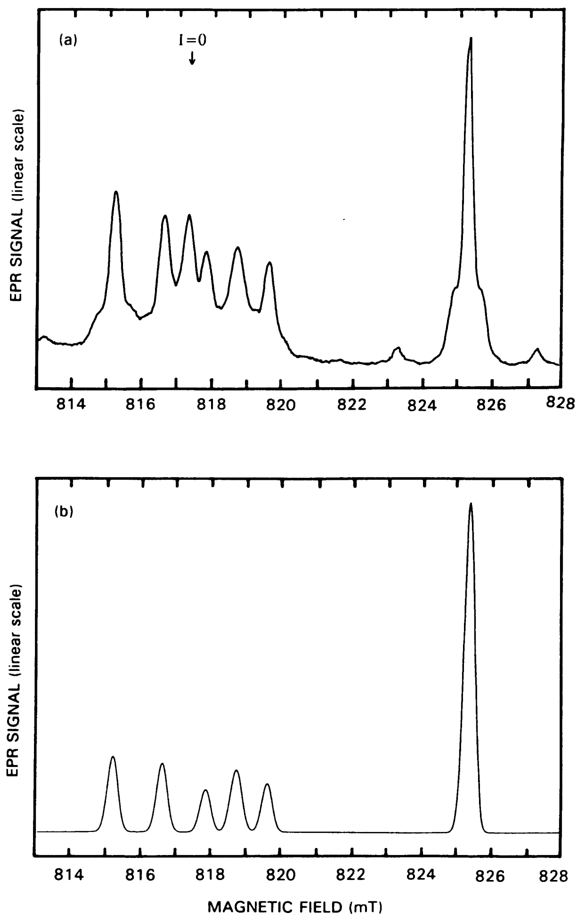

Fig. 2. EPR spectrum for **B** || [1 0 0]: (a) the experimental spectrum, (b) the simulated spectrum without ligand hyperfine interactions and without the central $I = 0$ component, calculated by superposing Gaussian lines of a width of 0.35 mT.

abundancy of 11.9%. In addition, a splitting due to the isotope ^{61}Ni, with nuclear spin $I = 3/2$, was observed at almost all magnetic field orientations. To illustrate the results some of the recorded spectra are shown in the Figs. 1 and 2a. Results of the complete angular dependence studies confirmed the orthorhombic symmetry of the centre. The branches forming the full pattern, each corresponding to specific orientations of the centre, are labelled A, B, C and D, following [4]; see also Fig. 4. For defect orientations A and B four hyperfine lines with equal intensities and with nearly equal separations were detected over most of the angular range. The splittings are largest in the [0 1 1] direction, as shown in Fig. 1a. The splitting decreases smoothly to zero in the [1 0 0] direction, where all hyperfine components are coincident and only one strong line is observed, as can be seen in Fig. 2a and in the computed Figs. 2b and 4. For the other orientations, C and D, the spectrum turns out to have more complexity, as demonstrated by the presence of extra lines at some angles. Differences in the intensity and unequal splitting between the components were observed, as illustrated in Figs. 1 and 2. In these figures the lines with label $I = 0$ belong to the spectra from the spin-zero nickel nuclei. A computer fit to the experimental data of the EPR spectrum was made using the spin Hamiltonian

$$H = \mu_B \mathbf{B} \cdot g \cdot \mathbf{S} - \mu_N \mathbf{B} \cdot g_N \cdot \mathbf{I} + \mathbf{S} \cdot A \cdot \mathbf{I} + \mathbf{I} \cdot Q \cdot \mathbf{I}, \qquad (1)$$

with electron spin $S = 1/2$ and nuclear spin $I = 3/2$. Data for the central $I = 0$ component were excluded from the fitting procedure. The first and second terms in equation (1) describe the electron and nuclear Zeeman interactions. The third and fourth ones correspond to the hyperfine and quadrupole nuclear interactions, respectively. The tensors g, g_N, A and Q are all constrained to have the orthorhombic-I symmetry. When using the isotropic g_N value of -0.4999, given by Fuller [5], in the computer fit, the lines corresponding to allowed transitions with $\Delta m_I = 0$ can well be fitted. Additional lines belonging

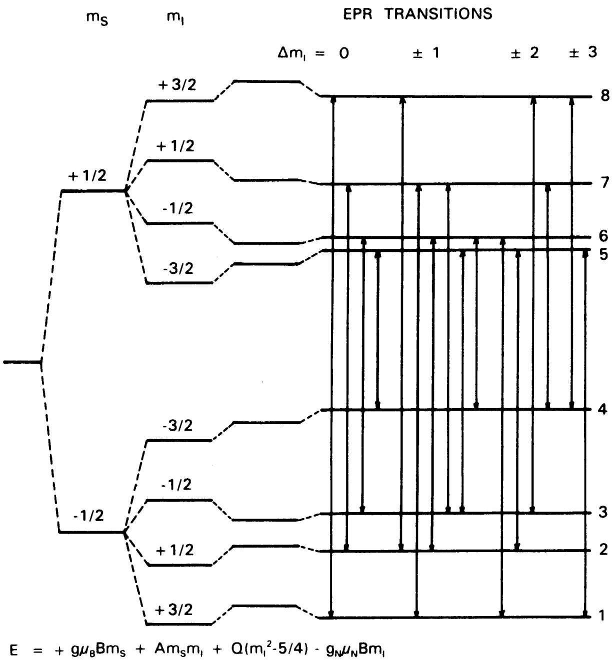

Fig. 3. The scheme of energy levels of the centre Si : $^{61}\text{Ni}_s^-$; $S = 1/2$, $I = 3/2$.

to transitions with $\Delta m_I \neq 0$, in the quantization scheme of Fig. 3, can be recognised. The presence of these "forbidden" transitions allows the determination of the purely nuclear Zeeman and quadrupole interactions in first order from the EPR spectrum. Including these forbidden lines in the fitting procedure, but keeping g_N fixed at its scalar value, results in an average deviation of 0.2 mT between calculated and experimental line positions. The best fit is significantly improved when using an anisotropic g_N instead of the scalar value. The maximum deviation between theoretical and experimental line positions in this case is not more than 60 μT. The spin Hamiltonian parameters obtained from the fit are given in Table 1 for the centre orientation A, which has the 2-fold axis along the $x = [1\,0\,0]$ direction.

With the spin Hamiltonian equation (1) and the parameters deduced from the fit, the simulation was made of the 16 EPR transitions indicated in Fig. 3. For all transitions the magnetic field position and transition probability were calculated for magnetic field directions in steps of 2 degrees in the range from the [1 0 0] to the [0 1 1] crystal direction. Figure 4 shows the angular dependence pattern plotted from these calculations including all EPR transitions exceeding a chosen threshold transition probability of 0.3. To illustrate the result, Fig. 2 shows two spectra for **B** ∥ [1 0 0]. Upper and lower parts in this figure are the measured and simulated parts, respectively. The simulated spectrum is based on calculated transition probabilities and on a superposition of Gaussian line shapes of a width of 0.35 mT, as observed in the experiments. In the simulation the component for the nickel isotopes with $I = 0$ as well as ligand hyperfine interactions with ^{29}Si are not included.

In order to explain the unusual splittings and the large differences in intensity between lines, the intensity plots were made for all EPR transitions of the four EPR orientations. For the orientation C the results are given in Fig. 5. Besides the four allowed lines corresponding to the transitions 1 ↔ 8, 2 ↔ 7, 3 ↔ 6 and 4 ↔ 5 with different intensities, there appear two forbidden $\Delta m_I = \pm 1$ lines with comparable intensity at positions between them. A similar behaviour of the allowed and forbidden transitions could be seen for the orientation D, but the two forbidden lines here have considerable intensity only in the region near the [1 0 0] and [0 1 1] directions. For both the orientations C and D the line intensities do not have a strong angular dependence. A different picture of transition probabilities is observed for the orientations A and B. The intensities of the four allowed transitions are strong and very much the same for **B** ∥ [0 1 1]. Towards lower angles they smoothly decrease to vanish at the [1 0 0] direction, where the line intensity is entirely due to several of the coinciding forbidden transitions with $\Delta m_I = \pm 1$, ± 2 and ± 3.

3.2. *Hyperfine interaction*

The interaction between the magnetic moment of a nucleus of spin I and the electrons with effective spin S contains information about the electronic distribution. In the conventional one-electron linear-combination-of-atomic-orbitals (LCAO) approximation, the wave function is written as the superposition of the electronic wave functions of *s*- and *d*-orbitals

$$\psi = \eta(\alpha\psi_s + \beta\psi_d). \tag{2}$$

Unpaired spin in the *s*- and *d*-orbitals is related to the isotropic and anisotropic parts, respectively, of the hyperfine interaction tensor A. For further analysis it is therefore convenient to decompose this tensor following

$$A = a\mathbb{1} + B, \tag{3}$$

where a is the trace of tensor A, and tensor B is traceless. The isotropic part is given by the spin density $\eta\alpha$ in the *s*-orbital by

$$a = (2/3)\mu_0 g\mu_B g_N \mu_N \eta^2\alpha^2|\Psi_s(0)|^2. \tag{4}$$

The dipole–dipole interaction with spin in *d*-orbitals is characterized by the axial tensor B with principal

Table 1. The principal values of the tensors of Si : Ni$_s^-$ *in the orientation* A. *The signs of tensors* A *and* Q *are given following the discussion in Sections* 3.2 *and* 3.3. *Data for some related orthorhombic centres are included*

Centre	Tensor	∥ [1 0 0]	∥ [0 1 1]	∥ [0 $\bar{1}$ 1]	Unit	Ref.
Si : ^{61}Ni$^-$	g	2.0163	2.0182	2.0536		[4]
	g_N	2.47	5.07	−2.35	MHz/T	This paper
	A	1.01	−39.98	−37.60	MHz	-
	a	−25.52	−25.52	−25.52	MHz	-
	B	26.53	−14.46	−12.08	MHz	-
	Q	2.42	2.09	−4.51	MHz	-
	Q^{us}	3.49	−1.90	−1.59	MHz	-
	Q^{vc}	−1.07	3.99	−2.92	MHz	-
Ge : ^{61}Ni$^-$	g	2.0294	2.0176	2.1128		[2]
	A	⩽4.8	36.7	30.9	MHz	-
Si : ^{105}Pd$^-$	g	2.0544	1.9715	1.9190		[1]
	g_N	−1.965	−1.917	2.105	MHz/T	[8]
	A	19.28	36.01	35.11	MHz	-
	Q	−12.975	15.850	−3.049	MHz	-
Si : OV$^-$	g	2.0033	2.0025	2.0093		[13]
	A	4.363	−0.997	5.593	MHz	[14]
	Q	0.149	0.174	−0.323	MHz	-
Si : V$^-$	g	2.0038	2.0028	2.0151		[11]

values $(2b, -b, -b)$ where

$$b = (1/4\pi)\mu_0 g\mu_B g_N\mu_N\eta^2\beta^2(\pm 2/7)\langle r^{-3}\rangle_d. \qquad (5)$$

In the analysis an axial form of hyperfine tensor is produced. Actually, the observed hyperfine tensor is very nearly axial along the [1 0 0] direction. The numerical analysis of the experimental hyperfine tensor A gives $a = \pm 25.52$ MHz and $b = \mp 13.27$ MHz. As the absolute signs of the spin Hamiltonian parameters are not determined in the EPR experiment, an ambiguity in the signs of a and b remains. However, in order to be consistent with the LCAO analysis, and taking account of the negative sign of g_N, a negative value for a and a positive value for b is assumed. The sign reversal of b, with respect to a, is appropriate for a d-orbital of the t_2-type [6]. Using atomic constants as given by Morton and Preston [6] and the isotropic nuclear g-value from Fuller [5], the spin density $\eta\alpha$ in the 4s orbital is determined as only 1.0%. The real value might be somewhat different as a result of polarisation of the 1s, 2s and 3s core shells. The spin density $\eta\beta$ in the 3d-orbital on the nickel atom is found to be 12.4%.

3.3. *Quadrupole interaction*

The quadrupole energy arises from the interaction between the nuclear quadrupole moment and the electric field gradient at the site of the nucleus. It depends on the unbalance of charge density associated with the defect. The contribution to the quadrupole interaction of a point charge $-e$ at a distance r from the nickel nucleus gives an axially symmetric quadrupole tensor with principal values $(2q, -q, -q)$, where

$$q = (-1/4\pi\varepsilon_0)[e^2Q/2I(I-1)](1/r^3). \qquad (6)$$

For nickel isotope ^{61}Ni, the nuclear spin $I = 3/2$; Q, the nuclear quadrupole moment, is taken from Fuller [5]. Calculating for the value $r = 2.35$ Å, which is the undistorted distance between the substitutional nickel atom and a nearest silicon site, one finds the value $q = -71.5$ kHz. Moving the Ni atom along the [1 0 0] axis to a minimum distance position with $r = 1.919$ Å raises the quadrupole parameter to $q = -131.4$ kHz. After application of the Sternheimer shielding correction factor of about 1.25, given by Childs and Goodman [7], the numbers obtained are still much smaller than the experimental values and can be neglected. The bigger measured effect must arise from unbalanced charges at the nucleus itself caused by electrons in d-orbitals. An electron in a d-orbital gives an axially symmetric quadrupole tensor with

$$q = (-1/4\pi\varepsilon_0)[e^2Q/2I(I-1)](\pm 2/7)\langle r^{-3}\rangle_d. \qquad (7)$$

As in equation (5) the sign ± depends on the specific d-orbital. For a free-atom d-orbital at the nickel site, the calculation gives the value $q = -(\pm)14.08$ MHz, which is the order of magnitude of the observed effect.

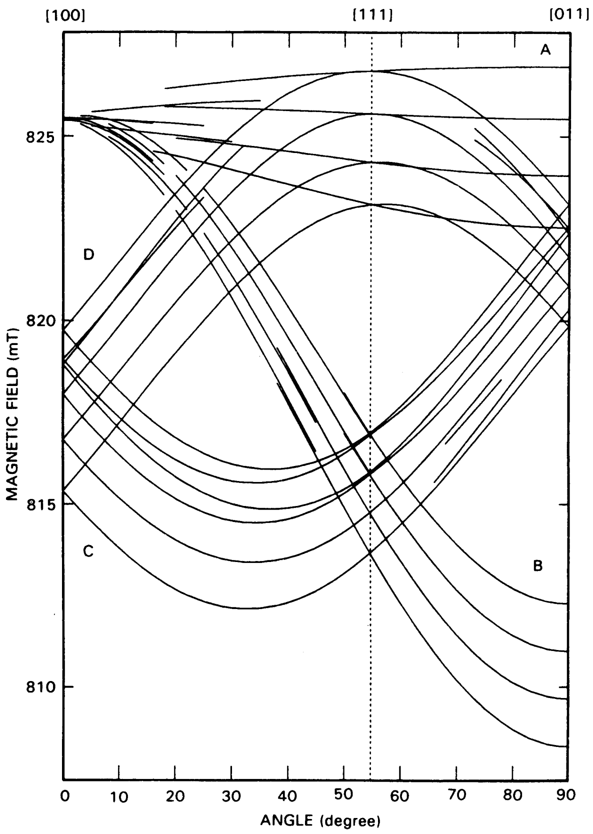

Fig. 4. The computed angular dependence of the EPR spectrum of Si : ^{61}Ni$_s^-$ without the central component arising from nickel nuclei of spin zero. In the plot, only resonances which have the relative intensity exceeding a threshold value of 0.3 are shown. The microwave frequency is 23.2909 GHz.

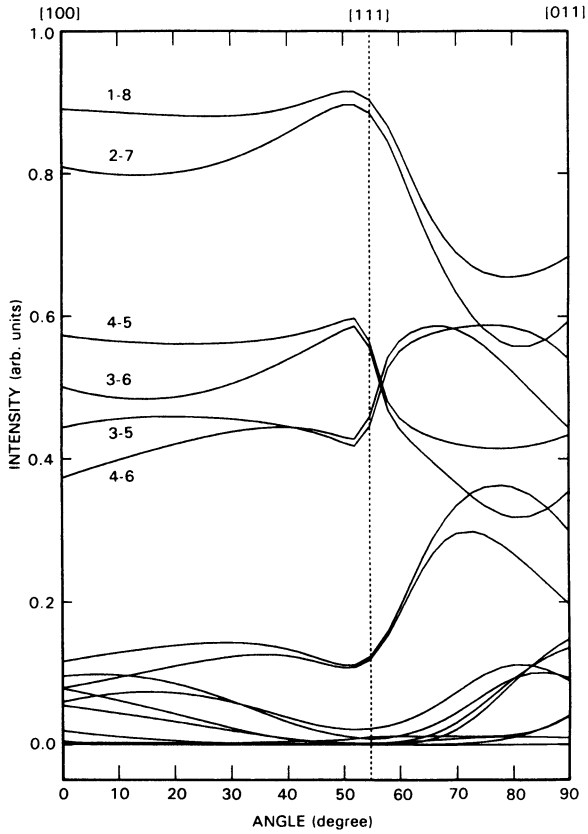

Fig. 5. Angular variation of line intensities for EPR orientation C.

For both hyperfine and quadrupole interactions, the mechanism of the interaction for an electron with unpaired spin (us) in a *d*-orbital is quite similar. One may thus derive the quadrupole tensor Q^{us} from the anisotropic hyperfine tensor B by a relation

$$Q^{us} = cB, \tag{8}$$

where the constant $c = q/b$ is determined by the comparison of the equations (5) and (7). For the present case $c = +0.1314$, leading to the principal values of the Q^{us} tensor as given in Table 1. As can be seen from the data, the contribution to the field gradient by the unpaired spin electron cannot explain the experimental data. It means that a contribution Q^{vc} resulting from valence electron charges at bonds must be present. The principal values of the required tensor can be obtained by subtracting Q^{us} from the experimental data. Although absolute signs of the parameters do not follow from the experiment, the relative signs of A and Q are fixed. Hence, having selected the proper signs of the hyperfine parameters, as discussed in the previous section, the absolute values for the quadrupole interaction follow, as included in Table 1. The result for Q^{vc}, as given in Table 1, is a tensor with approximate [0 1 1] axial symmetry and $q \approx 2$ MHz. It corresponds to about 14% of an electron.

4. DISCUSSION

In this paper and in previous ones the hyperfine and quadrupole parameters were reported for the centre Si : Ni$_s^-$ [4] and the related centres Si : Pd$_s^-$ [1, 8], Si : Pt$_s^-$ [1] and Ge : Ni$_s^-$ [2]. Measurements have included the impurity self interactions and the ligand interactions with ^{29}Si or ^{73}Ge host nuclei. To account for the electronic structure of these substitutional impurity centres some models were proposed.

In the model as used successfully by Ludwig and Woodbury to describe 3*d*-transition metals, the impurities are fully tetrahedrally bonded to four nearest neighbour silicon atoms [9]. In this case the negative substitutional nickel would have 7 electrons in the 3*d* shell, predicting cubic symmetry, spin $S = 3/2$, isotropic hyperfine interaction and no quadrupole effect. This all is at variance with the experimental findings.

In the vacancy model proposed more recently by Watkins for the late transition elements, the impurity has a closed *d*-shell and is accommodated in a negative vacancy [10]. Having the closed *d*-shell, the transition metal impurities are expected to have a small effect on the electronic properties. The unpaired electron will occupy an anti-bonding orbital, of symmetry type b_1, between two silicon next-nearest neighbour atoms [11]. The features as characteristic for the vacancy are apparently reproduced for the negative substitutional oxygen impurity [12]. For this centre the g-values, ligand hyperfine interactions and symmetry type of the unpaired spin orbital, are close to or identical to that of the vacancy [13, 14]. For the transition element impurities the situation appears, however, to be more complex.

Just recently, electronic structure calculations for Ni^-, Pd^- and Pt^- in silicon were made by Delerue *et al.* [15] in order to examine the validity of the models. In these calculations, the unpaired spin electron of the centre is considered to be in the b_1 anti-bonding orbital, as in the case of the vacancy, and an admixture of the *d* impurity states into the vacancy wave function is taken into account. The calculation of the localisation factor γ^2 of the wave functions on the impurity atom gives the values 0.17, 0.15 and 0.13 for Ni^-, Pd^- and Pt^-, respectively. From the fact that a good fit could be obtained for the g and A values for Pt^- using this localisation, the vacancy model was concluded to be valid for these centres. The theoretical value $\gamma^2 = 0.17$ for nickel is rather well confirmed by the experimental value 0.13 following from the analysis of the hyperfine interaction presented in Section 3.2. Nevertheless, upon closer inspection of the EPR data, in particular the hyperfine parameters, one may recognise basic differences in the vacancy and transition metal structure. As can be seen in Table 1, the self hyperfine interaction in the oxygen-vacancy complex gives the tensor A nearly axially symmetric around the [0 1 1] direction, satisfying the requirement of the b_1 type orbital, with spin densities in the s- and p-orbitals on the oxygen atom of about 1.2%. By contrast, the hyperfine tensors of the $\mathrm{Si:Ni}_s^-$ centre, and also of $\mathrm{Ge:Ni}_s^-$ and $\mathrm{Si:Pd}_s^-$, are nearly axial around [1 0 0] and the localisations of the paramagnetic electrons in the s- and d-orbitals on the impurity atom are found to be at least ten times bigger than that of the oxygen centre. From the nearly perfect axial symmetry around [1 0 0] one must conclude that the spin is described mainly by an a_1 or a_2 type orbital on the nickel impurity. The high localisation excludes b_1 and a_2 orbitals, as these have one or two nodal planes with vanishing wave functions and contact hyperfine interactions. In this way, the observed hyperfine angular dependence is directly related to the compulsary choice for an a_1 symmetry type orbital. It presents rather clear evidence of differences in the microscopic structure of the vacancy and the transition impurity. In support of this different structure, the quadrupole interaction as monitored by $^{17}\mathrm{O}$ in $\mathrm{Si:OV}^-$ is very small compared to the case of $^{61}\mathrm{Ni}$ in $\mathrm{Si:Ni}_s^-$. It is indicative for a larger redistribution of charge around the centre in the transition element case and different aspects of bonding. Obviously, the g tensors of the transition element impurities differ substantially from the pure spin value $g = 2.0023$, typical for the vacancy and vacancy-model centres, with quenching of the orbital contribution. Also, within the group of transition elements the g values vary widely from the lighter to the heavier ones, suggesting the effectiveness of spin–orbit interaction. The involvement of *d*-orbitals seems to be rather different in the various cases. One may conclude that both in electric and magnetic properties the transition elements, if inspected in sufficient detail, reveal clear impurity dependent behaviour.

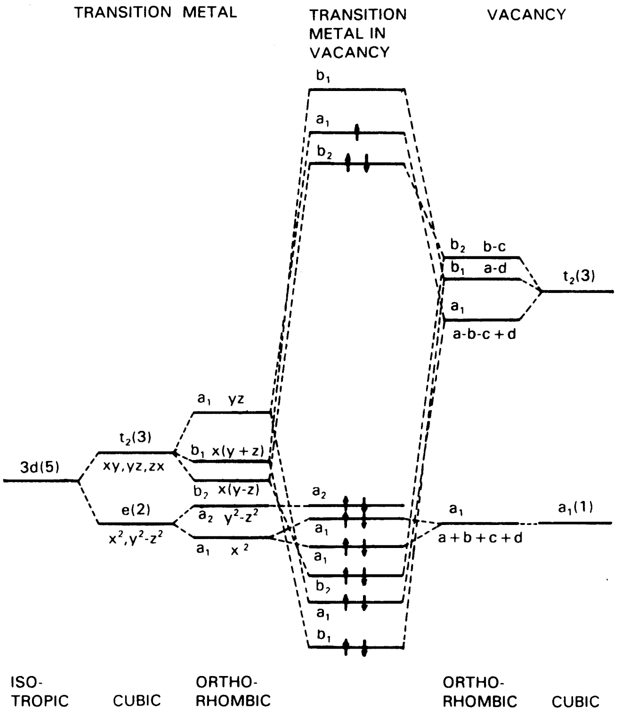

Fig. 6. The scheme of energy levels in the case of an interaction between the transition impurity and the lattice vacancy.

These findings can be represented in the electronic structure diagram of Fig. 6 and the geometrical atomic model of Fig. 7. The figures depict the defect in

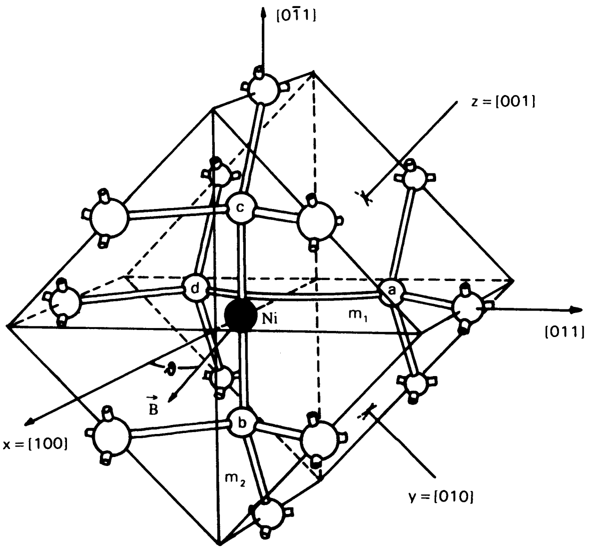

Fig. 7. A model for the centre Si : Ni$_s^-$ in which the transition metal is bound to two silicon neighbours.

orientation A and include the definition of coordinate axes. In the left part of Fig. 6 *d*-electron states of nickel with corresponding energy levels are shown. The vacancy related dangling bond states are given to the right. As illustrated in the diagram the properties of the substitutional impurity are determined by the interaction between t_2 states of vacancy and impurity. In the orthorhombic symmetry of the centre the t_2 degeneracy is lifted into singlet a_1, b_1 and b_2 states. The interaction of these levels gives an appreciable bonding-antibonding splitting. In the negative charge state of the defect, 15 electrons are to be accommodated in these levels. By having the ordering of levels as indicated, the unpaired spin electron will be in a a_1 state, as required by the experimental result. The analysis gives about 15% nickel part and a remaining 85% silicon part in the wave function. To account for the quadrupole interaction, one notes that 12 electrons with lowest energy form a closed shell configuration and do not contribute to an electric field gradient at the nickel site. In addition to the unpaired a_1 electron two electrons in the next lower b_2 state are expected to have a noticeable effect, consistent with the analysis described in Section 3.3. From the b_2 symmetry one concludes that the nearest neighbour sites *b* and *c* are involved in this orbital. It reflects a predominant bonding with these two atoms. A model in which bonding between the transition element and two neighbour silicon atoms was emphasized has been proposed earlier [16]. An illustration of such model is given in Fig. 7.

REFERENCES

1. H.H. Woodbury & G.W. Ludwig, *Phys. Rev.* **126**, 466 (1962).
2. G.W. Ludwig & H.H. Woodbury, *Phys. Rev.* **113**, 1014 (1959).
3. L.S. Vlasenko, A.A. Lebedev, E.S. Taptygov & V.A. Khramtsov, *Sov. Tech. Phys. Lett.* **13**, 553 (1987). [Translated from *Pis'ma Zh. Tekh. Fiz.* (*USSR*) **13**, 1322 (1987)].
4. L.S. Vlasenko, N.T. Son, A.B. van Oosten, C.A.J. Ammerlaan, A.A. Lebedev, E.S. Taptygov & V.A. Khramtsov, *Solid State Commun.* **73**, 393 (1990).
5. G.H. Fuller, *J. Phys. Chem. Ref. Data* **5**, 835 (1976).
6. J.R. Morton & K.F. Preston, *J. Magn. Reson.* **30**, 577 (1978).
7. W.J. Childs & L.S. Goodman, *Phys. Rev.* **170**, 136 (1968).
8. A.B. van Oosten, N.T. Son, L.S. Vlasenko & C.A.J. Ammerlaan, *Materials Science Forum* **38–41**, 355 (1989).
9. G.W. Ludwig & H.H. Woodbury, *Phys. Rev. Lett.* **5**, 98 (1960).
10. G.D. Watkins *Physica* **117B&118B**, 9 (1983).
11. M. Sprenger, S.H. Muller, E.G. Sieverts & C.A.J. Ammerlaan, *Phys. Rev.* **B35**, 1566 (1987).
12. G.D. Watkins & J.W. Corbett, *Phys. Rev.* **121**, 1001 (1961).
13. R. van Kemp, E.G. Sieverts & C.A.J. Ammerlaan, *Phys. Rev.* **B40**, 4037 (1989).
14. R. van Kemp, M. Sprenger, E.G. Sieverts & C.A.J. Ammerlaan, *Phys. Rev.* **B40**, 4054 (1989).
15. C. Delerue, F.G. Anderson & M. Lannoo, in *The Physics of Semiconductors* (Edited by E.M. Anastassakis and J.D. Joannopoulos), World Scientific, Singapore (1990), p. 585.
16. C.A.J. Ammerlaan & A.B. van Oosten, *Phys. Scripta* **T25**, 342 (1989).